Theory and Design of Low-Insertion Loss Fin-Line Filters

FRITZ ARNDT, JENS BORNEMANN, DIETRICH GRAUERHOLZ, AND RÜDIGER VAHLDIECK

Abstract—**A design theory is described for low-insertion loss fin-line filters that includes both higher order mode propagation and finite thickness of the dielectric substrate and the metallic fins. Design data for three-resonator type fin-line filters with several substrate thicknesses are given for midband frequencies of about 15, 34, and 66 GHz. The measured insertion losses in the passband are 0.25, 0.5, and 1.3 dB, respectively, for these three frequencies.**

I. Introduction

INTEGRATED FIN-LINE is a very attractive medium for millimeter-wave applications [1]–[11]. The advantages of these circuits include the potential of low-insertion loss designs, if extremely high gap widths $g/b=1$ (Fig. 1) are taken into account [2]. This paper introduces a design theory for such fin-line filters.

For three-dimensional fin-line structures, so far, only experimental data and first-order theories ([2]–[7]) are available with considerable restrictions on the low loss design. In [2] and [3], the higher order mode coupling is neglected in the analysis of fin-line discontinuities. A combination of the coupled-mode technique accompanied by a spectral domain solution is used in [4], but this theory is only valid as long as there is simply a gradual change of line discontinuities in the direction of propagation. In [5]–[7], the hybrid modes of the fin-line cross section are calculated under the assumption that the thickness of the substrate is very small in comparison with the waveguide width. The influence of the finite thickness of the dielectric as well as of the copper cladding, however, cannot be neglected, since it plays a significant role concerning midband insertion loss, stopband attenuation, and midband frequency.

Fin-line filter cross sections with extremely high gap width $g/b=1$ (Fig. 1(b)) do not require fin-line solutions like in [8]–[11]. For the field theory treatment given in this paper, the high-Q fin-line filter (Fig. 1(b)) is regarded as consisting of alternating waveguide structures: a waveguide with a dielectric slab and three parallel waveguides, the middle of which is filled with dielectric (Fig. 2(a)). The method of orthogonal expansion into suitable eigenmodes [12] is used together with the field matching at the steps investigated. This allows consideration of the higher order mode excitation up to a desired number of modes, the finite thickness of the substrate and metallic fins, and the sudden changes in the gapwidths.

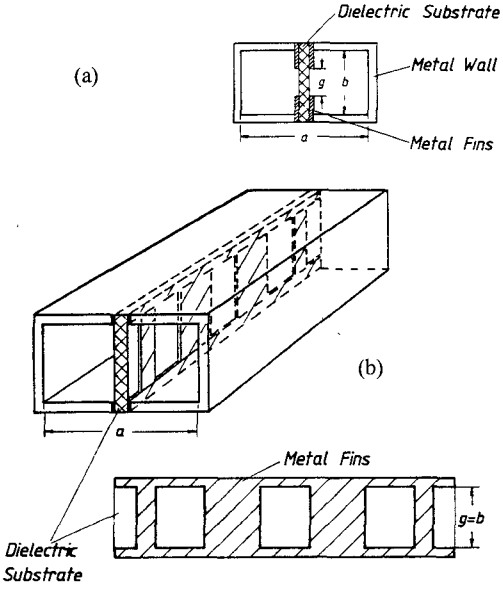

Fig. 1. Fin-line configuration. (a) General cross section with bilateral grounded fins. (b) Low insertion loss fin-line filter structure.

The theory is verified by measurements. The measured frequency response of the fin-line filters that have been designed and operated at about 15, 34, and 66 GHz shows good agreement between theory and practical results. The high-Q design leads to passband insertion losses of typically only 0.25, 0.5, and 1.3 dB, respectively, at these three frequencies.

II. Theory

A. Scattering Matrix of the Three-Waveguide Structure of Finite Length within a Waveguide

For each subregion[1] $\nu=$ I, II, III, IV (Fig. 2(b)) the fields are derived from the x-component of the vector potential Q which is assumed to be a sum of suitable eigenmodes

$$Q_x^\nu = \sum_{m=1}^{\infty} A_m^\nu \sin\left(\frac{m\pi}{p^\nu} f^\nu\right) \cdot e^{-jk_{zm}^\nu \cdot z}. \tag{1}$$

(p^ν, f^ν, and k_{zm}^ν are explained in the Appendix.) The

Manuscript received July 7, 1981; revised September 3, 1981.

The authors are with the Microwave Department, University of Bremen, Kufsteiner Str., NW 1, D-2800 Bremen, 33, West Germany.

[1]The analysis is given for the general case of structures placed unsymmetrically in the E-plane of rectangular wave-guides to include possible applications of the dielectric slab structure as phase shifters.

0018-9480/82/0200-0155$00.75 ©1982 IEEE

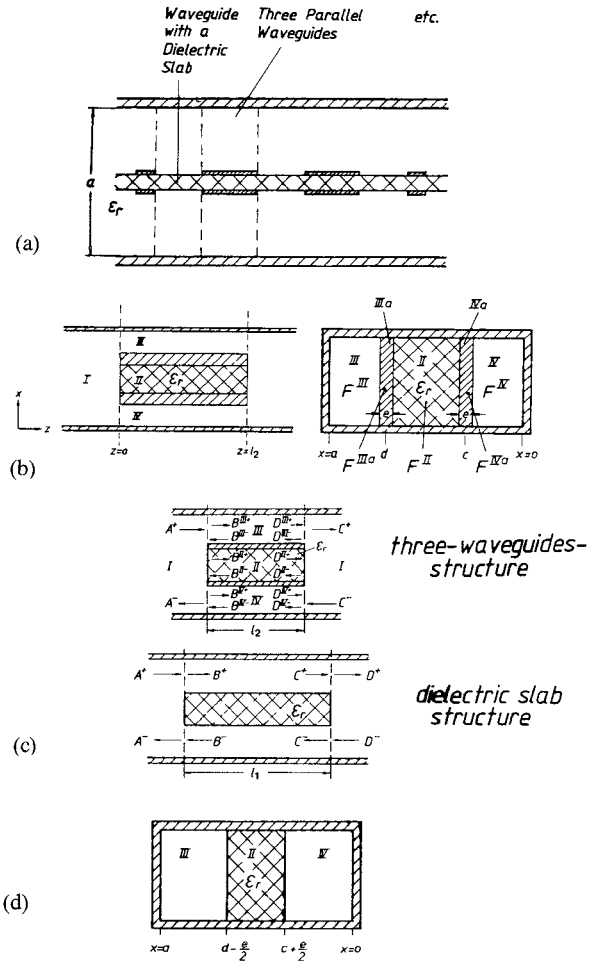

Fig. 2. Configuration for the field-theory treatment. (a) Alternating waveguide structures. (b) Transition to three parallel waveguides. (c) Wave amplitude vectors of the structures of finite length. (d) Transition to dielectric slab structure.

coefficients A_m^ν are normalized to the related power

$$P_m^\nu = \int_{F^\nu} E \times H^* dF = 1W. \tag{2}$$

The components of the electromagnetic field are calculated by

$$E_x^\nu = 0 \qquad H_x^\nu = k^{\nu 2} Q_x^\nu + \frac{\delta^2 Q_x^\nu}{\delta x^2}$$

$$E_y^\nu = -j\omega\mu \frac{\delta Q_x^\nu}{\delta z} \qquad H_y^\nu = \frac{\delta^2 Q_x^\nu}{\delta x \delta y}$$

$$E_z^\nu = j\omega\mu \frac{\delta Q_x^\nu}{\delta y} \qquad H_z^\nu = \frac{\delta^2 Q_x^\nu}{\delta x \delta z} \tag{3}$$

where

$$k^{\nu 2} = \omega^2 \mu_0 \epsilon_\nu \qquad \epsilon_\nu = \epsilon_0 \cdot \epsilon_r^{(\nu)}.$$

By matching the field components at the corresponding interfaces F^ν of the adjacent subregions (Fig. 2(b)) at $z = 0$ and $z = l_2$

$$E_y^{\mathrm{I}} = \begin{Bmatrix} E_y^{\mathrm{II}} & (x,y) \in F^{\mathrm{II}} \\ E_y^{\mathrm{III}} & (x,y) \in F^{\mathrm{III}} \\ E_y^{\mathrm{IV}} & (x,y) \in F^{\mathrm{IV}} \\ 0 & (x,y) \in F^{\mathrm{IIIa}} \\ 0 & (x,y) \in F^{\mathrm{IVa}} \end{Bmatrix}$$

$$H_x^{\mathrm{I}} = \begin{Bmatrix} H_x^{\mathrm{II}} & (x,y) \in F^{\mathrm{II}} \\ H_x^{\mathrm{III}} & (x,y) \in F^{\mathrm{III}} \\ H_x^{\mathrm{IV}} & (x,y) \in F^{\mathrm{IV}} \end{Bmatrix} \tag{4}$$

the coefficients A_m^ν in (1) can be determined after multiplication with the appropriate orthogonal function related to each subregion. This leads to the coupling integrals elucidated in the Appendix.

If the forward and backward waves at the two steps (Fig.

2(c)) of the structure of finite length l_2 are suitably related together, then (1)–(4) can be written as the desired scattering matrix

$$\begin{pmatrix}(A)^-\\(C)^+\end{pmatrix}=\begin{pmatrix}(S_{11}) & (S_{12})\\(S_{21}) & (S_{22})\end{pmatrix}\begin{pmatrix}(A)^+\\(C)^-\end{pmatrix} \tag{5}$$

with

$$(S_{11})=(S_{22})=(W)^{-1}\{[(U)+(E)]^{-1}(V)[(U)+(E)]^{-1}(V)-[(U)+(E)]^{-1}[(U)-(E)]\}$$
$$(S_{12})=(S_{21})=(W)^{-1}\{[(U)+(E)]^{-1}(V)-[(U)+(E)]^{-1}(V)[(U)+(E)]^{-1}[(U)-(E)]\}. \tag{6}$$

The abbreviations are explained in the Appendix.

B. Scattering Matrix of the Dielectric-Slab Structure of Finite Length within a Waveguide

For this structure (Figs. 2(c), (d)) the waves in regions[2] I, II, III, and IV are expanded into the eigenmodes

$$E_y^{\mathrm{I}}=-\omega\mu\sum_{m=1}^{\infty}k_{zm}^{\mathrm{I}}A_m^{\mathrm{I}}\sin\frac{m\pi}{a}x\cdot e^{-jk_{zm}^{\mathrm{I}}z}$$
$$H_x^{\mathrm{I}}=\sum_{m=1}^{\infty}k_{zm}^{\mathrm{I2}}A_m^{\mathrm{I}}\sin\frac{m\pi}{a}x\cdot e^{-jk_{zm}^{\mathrm{I}}z}$$
$$H_z^{\mathrm{I}}=-j\sum_{m=1}^{\infty}\frac{m\pi}{a}k_{zm}^{\mathrm{I}}A_m^{\mathrm{I}}\cos\frac{m\pi}{a}x\cdot e^{-jk_{zm}^{\mathrm{I}}z} \tag{7a}$$

$$E_y^{\mathrm{II}}=-\omega\mu\sum_{m=1}^{\infty}k_{zm}\left(A_m^{\mathrm{II}}\cos\left(k_{xm}^{\mathrm{II}}\cdot x\right)+B_m^{\mathrm{II}}\sin\left(k_{xm}^{\mathrm{II}}\cdot x\right)\right)e^{-jk_{zm}z}$$
$$H_z^{\mathrm{II}}=-j\sum_{m=1}^{\infty}k_{zm}k_{xm}^{\mathrm{II}}\left(-A_m^{\mathrm{II}}\sin\left(k_{xm}^{\mathrm{II}}\cdot x\right)+B_m^{\mathrm{II}}\cos\left(k_{xm}^{\mathrm{II}}\cdot x\right)\right)e^{-jk_{zm}z}$$
$$H_x^{\mathrm{II}}=\sum_{m=1}^{\infty}\left(k^{\mathrm{II2}}-k_{xm}^{\mathrm{II2}}\right)\left(A_m^{\mathrm{II}}\cos\left(k_{xm}^{\mathrm{II}}\cdot x\right)+B_m^{\mathrm{II}}\sin\left(k_{xm}^{\mathrm{II}}\cdot x\right)\right)e^{-jk_{zm}z} \tag{7b}$$

$$E_y^{\mathrm{III}}=-\omega\mu\sum_{m=1}^{\infty}k_{zm}A_m^{\mathrm{III}}\left(-\tan\left(k_{xm}^{\mathrm{III}}\cdot a\right)\cos\left(k_{xm}^{\mathrm{III}}\cdot x\right)+\sin\left(k_{xm}^{\mathrm{III}}\cdot x\right)\right)e^{-jk_{zm}z}$$
$$H_z^{\mathrm{III}}=-j\sum_{m=1}^{\infty}k_{zm}k_{xm}^{\mathrm{III}}A_m^{\mathrm{III}}\left(\tan\left(k_{xm}^{\mathrm{III}}\cdot a\right)\sin\left(k_{xm}^{\mathrm{III}}\cdot x\right)+\cos\left(k_{xm}^{\mathrm{III}}\cdot x\right)\right)e^{-jk_{zm}z}$$
$$H_x^{\mathrm{III}}=\sum_{m=1}^{\infty}\left(k^{\mathrm{III2}}-k_{xm}^{\mathrm{III2}}\right)A_m^{\mathrm{III}}\left(-\tan\left(k_{xm}^{\mathrm{III}}\cdot a\right)\cos\left(k_{xm}^{\mathrm{III}}\cdot x\right)+\sin\left(k_{xm}^{\mathrm{III}}\cdot x\right)\right)\cdot e^{-jk_{zm}z} \tag{7c}$$

$$E_y^{\mathrm{IV}}=-\omega\mu\sum_{m=1}^{\infty}k_{zm}A_m^{\mathrm{IV}}\sin\left(k_{xm}^{\mathrm{IV}}\cdot x\right)\cdot e^{-jk_{zm}z}$$
$$H_z^{\mathrm{IV}}=-j\sum_{m=1}^{\infty}k_{zm}k_{xm}^{\mathrm{IV}}A_m^{\mathrm{IV}}\cos\left(k_{xm}^{\mathrm{IV}}\cdot x\right)\cdot e^{-jk_{zm}z}$$
$$H_x^{\mathrm{IV}}=\sum_{m=1}^{\infty}\left(k^{\mathrm{IV2}}-k_{xm}^{\mathrm{IV2}}\right)A_m^{\mathrm{IV}}\sin\left(k_{xm}^{\mathrm{IV}}\cdot x\right)\cdot e^{-jk_{zm}z}. \tag{7d}$$

The common propagation factor k_{zm} in regions II, III, and IV is determined by the boundary conditions along the dielectric slab

$$\left.\begin{aligned}E_y^{\mathrm{II}}&=E_y^{\mathrm{IV}}\\H_z^{\mathrm{II}}&=H_z^{\mathrm{IV}}\end{aligned}\right|_{x=c+\frac{e}{2}}\qquad\left.\begin{aligned}E_y^{\mathrm{II}}&=E_y^{\mathrm{III}}\\H_z^{\mathrm{II}}&=H_z^{\mathrm{III}}\end{aligned}\right|_{x=d-\frac{e}{2}}. \tag{8}$$

With (7(a–d)), a system of linear equations is obtained where the determinant is required to be zero. This leads to a transcendental equation for the propagation factor k_{zm} which is solved numerically

$$\frac{1}{k_{xm}^{\mathrm{II}}}\cdot\tan\left(k_{xm}^{\mathrm{II}}(d-c-e)\right)+\frac{1}{k_{xm}^{\mathrm{III}}}\cdot\tan\left(k_{xm}^{\mathrm{III}}\left(a-d+\frac{e}{2}\right)\right)+\frac{1}{k_{xm}^{\mathrm{IV}}}\cdot\tan\left(k_{xm}^{\mathrm{IV}}\cdot\left(c+\frac{e}{2}\right)\right)$$
$$-\frac{k_{xm}^{\mathrm{II}}}{k_{xm}^{\mathrm{III}}\cdot k_{xm}^{\mathrm{IV}}}\tan\left(k_{xm}^{\mathrm{II}}(d-c-e)\right)$$
$$\cdot\tan\left(k_{xm}^{\mathrm{III}}\left(a-d+\frac{e}{2}\right)\right)\tan\left(k_{xm}^{\mathrm{IV}}\cdot\left(c+\frac{e}{2}\right)\right)=0 \tag{9}$$

where the relation holds

$$\begin{bmatrix}k_{xm}^{\mathrm{II2}}\\k_{xm}^{\mathrm{III2}}\\k_{xm}^{\mathrm{IV2}}\end{bmatrix}=\begin{bmatrix}k_0^2\cdot\epsilon_r\\k_0^2\\k_0^2\end{bmatrix}-k_{zm}^2,\qquad k_0^2=\omega^2\mu_0\epsilon_0. \tag{10}$$

The scattering matrix S of the structure of finite length l_1 (Fig. 2(c)) is given by

$$\begin{pmatrix}(A)^-\\(D)^+\end{pmatrix}=\begin{pmatrix}(S_{11}) & (S_{12})\\(S_{21}) & (S_{22})\end{pmatrix}\begin{pmatrix}(A)^+\\(D)^-\end{pmatrix} \tag{11}$$

[2]See footnote 1.

TABLE I
COMPUTER OPTIMIZED DESIGN DATA FOR LOW-INSERTION LOSS FIN-LINE FILTERS (DIELECTRIC MATERIAL: RT/DUROID 5880 $\epsilon_r = 2.22$; COPPER CLADDING THICKNESS $e = 17.5\ \mu$m (INCLUDED IN THE COMPUTATIONS))

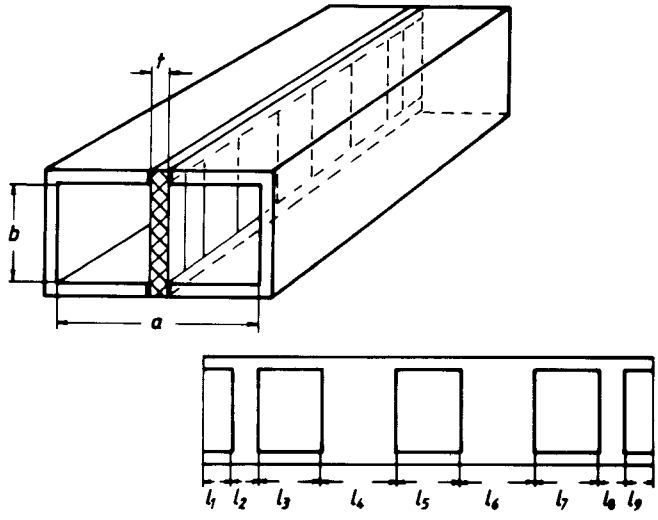

Fin-line Filter	Substrate thickness t	$l_1=l_9$ mm	$l_2=l_8$ mm	$l_3=l_7$ mm	$l_4=l_6$ mm	l_5 mm	f_o GHz	Bandwidth $\Delta f^{*)}$ MHz
Ku-band a=15.799mm b= 7.899mm	0.005"	27.079	2.178	8.390	8.148	8.400	15.19	560
	0.01"	27.565	2.075	8.400	7.760	8.400	15.285	601
	0.02"	28.127	1.976	8.350	7.372	8.350	15.252	560
	1/32"	13.706	1.860	8.300	6.984	8.300	15.207	557
	1/16"	15.660	1.500	8.000	5.840	8.000	15.190	524
Ka-band a=7.112mm b=3.556mm	0.005"	19.5575	0.715	3.740	4.115	3.745	34.02	620
	0.01"	19.928	0.660	3.740	3.800	3.745	33.989	698
	0.02"	20.580	0.550	3.630	3.420	3.640	33.982	675
	1/32"	21.260	0.480	3.525	2.970	3.530	33.99	635
V-band a=3.76mm b=1.88mm	0.005"	14.770	0.347	1.895	2.038	1.900	66.09	1055
	0.01"	14.824	0.353	1.855	2.038	1.860	65.940	1080

*) 3dB limits

with

$$(S_{11}) = (S_{22}) = (Q_{11}) + (Q_{12})(R)(W)(Q_{22})(R)(Q_{21})$$
$$(S_{12}) = (S_{21}) = (Q_{12})(R)(W)(Q_{21}). \quad (12)$$

The abbreviations are explained in the Appendix.

The scattering matrix of the total fin-line filter structure is obtained by suitably combining the transitions, the length of waveguide I (Fig. 2(b)) being reduced to zero if structures A and B (or inverse) are joined together directly. For the computer calculation the expansion into twenty eigenmodes in every region has turned out to be sufficient.

III. DESIGN

Fin-line filters of the three-resonator type (that means with four metal inserts) for midband frequencies of about 15, 34, and 66 GHz are chosen for design examples. The corresponding waveguide housings are WR 62 (*Ku*-band, $a = 15.799$ mm, $b = 7.899$ mm), WR 28 (*Ka*-band, $a = 7.112$ mm, $b = 3.556$ mm), and WR 15 (*V*-band, $a = 3.76$ mm, $b = 1.88$ mm).

RT/duroid 5880 ($\epsilon_r = 2.22$) has turned out to be a relatively cheap substrate material with sufficiently good electrical properties; the chosen substrate thicknesses t commercially available are 0.005 in, 0.01 in, 0.02 in, 1/32 in, 1/16 in Rexolite ($\epsilon_r = 2.54$), and Polyguide ($\epsilon_r = 2.32$) have also been investigated for substrate materials showing similar results.

The design process is started with filter dimensions given in [5], [6] for the narrow slot filter ($g \ll b$, Fig. 1), which exhibits a relatively poor measured insertion loss (e.g., about 2 dB for a midband frequency of about 15 GHz.) An optimizing computer program is used [13] and [14], which varies the parameters l_2 to l_5 (Table I) for the given thickness of the dielectric and of the copper cladding, as

well as for the roughly fixed midband frequency and 3-dB bandwidth, until the insertion loss within the passband yields a minimum and the stopband attenuation an optimum. ($l_1 = l_9$ is determined by the chosen total length of the dielectric substrate due to the measuring housing.) The evolution strategy [13], [14] was applied instead of, for instance, the Fletcher–Powell method, because no differentiation step in the optimizing process is necessary, which reduces the involved computing time. This was further reduced by including some physical considerations into the optimization process: the dimensions $l_3 = l_7$ and l_5 of the resonator sections determine essentially the midband frequency f_0, the widths of the metal fin bridges determine essentially the ripple of the passband insertion loss. Because the midband frequency was assumed to be not so critical, merely coarse steps were foreseen for the resonator sections. The total computing time for the optimization process of one set of filter parameters was about 20–30 min. A SIEMENS-7880 computer was used for the computations.

Table I shows the computed data of the optimized low-insertion loss fin-line filters. For the *Ku*-band design all commercially available substrate thicknesses for RT/duroid 5880 material were considered. For the *Ka*-band and the *V*-band design the thicker substrates were not taken into account. This is because the related stopband attenuation is reduced considerably if the substrate is thicker than about one quarter-wavelength, allowing an important amount of power to be propagated directly across the dielectric slab.

The finite thickness of the metallization is also included in the computations. The neglect of the metallization influence would mainly lead to incorrect calculations of the midband frequency (e.g., for the *Ka*-band filters the error would be about 400 MHz).

To reduce the influence of etching errors, the copper cladding thickness should be as thin as possible. For the chosen substrate, however, only a thickness of 17.5 μm was commercially available. Further investigations will include Quartz substrates with about 5-μm gold cladding.

Since its fundamental mode differs scarcely from the fundamental TE_{10}-waveguide mode the low-insertion loss filter requires no tapered transitions to the waveguide. Further, the designed filter section begins and ends with the dielectric slab and not with the metallized inserts. Besides the above mentioned practical advantage of standardized substrate lengths this choice, in addition, reduces the already low matching loss.

IV. Results

Fig. 3 shows the calculated and measured insertion-loss (scattering coefficient S_{21}) in decibels as a function of frequency for three-resonator *Ku*-band fin-line filters with substrate thicknesses of 0.01 in and 1/16 in. The calculated minimum insertion losses in the passband are about 0.1 dB for both examples, which indicates the very low matching losses for both substrate thicknesses. The corresponding measured values are about 0.25 and 0.6 dB, respectively.

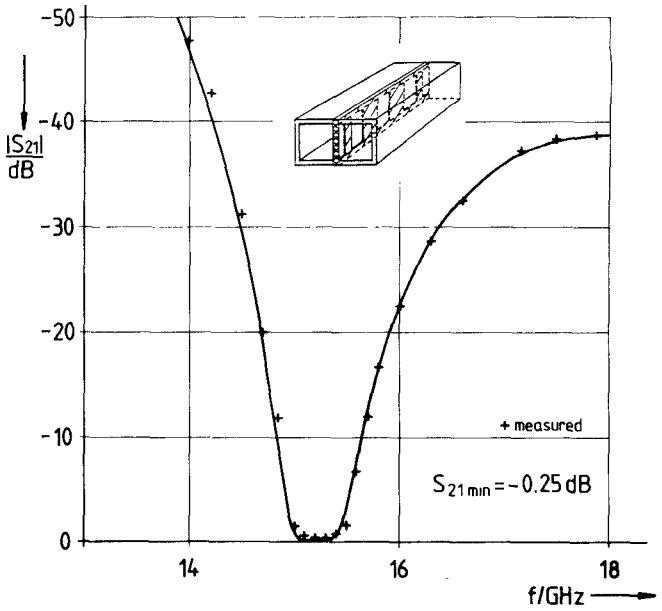

(a)

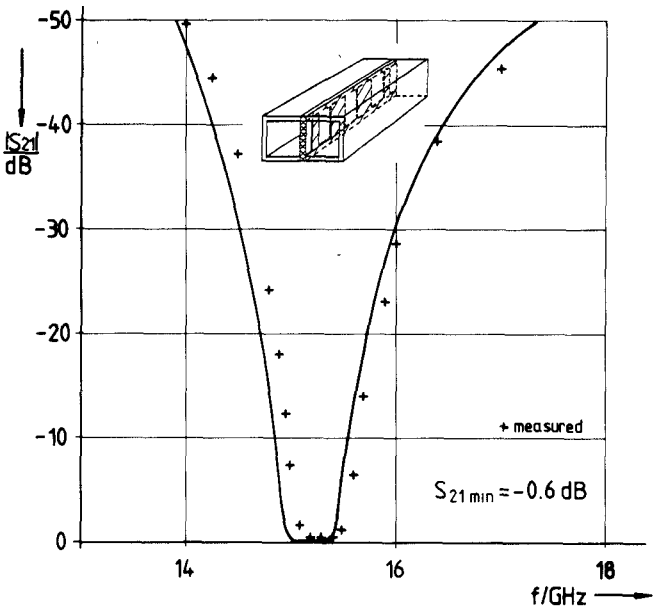

(b)

Fig. 3 Calculated and measured insertion loss of *Ka*-band fin-line filters (Table I). (a) Thickness of the dielectric substrate: 0.01 in. (b) Thickness of the dielectric substrate: 1/16 in

These results compare well with the low experimental insertion loss of the inductive strip bandpass filter [15].

The comparison of the two filter responses of Fig. 3 shows that the thicker substrate provides better stopband attenuation,[3] but the measured passband insertion loss is also higher because of the higher amount of energy within the wider lossy dielectric. The dielectric losses are not included in the computations.

[3] This is because the reduction of the space between the metallic inserts and the waveguide sidewalls increases the cutoff frequency of the first higher order filter mode. On the other hand this allows increased power propagation directly across the dielectric slab. Therefore, the upper limit are substrate thicknesses of about one quarter-wavelength.

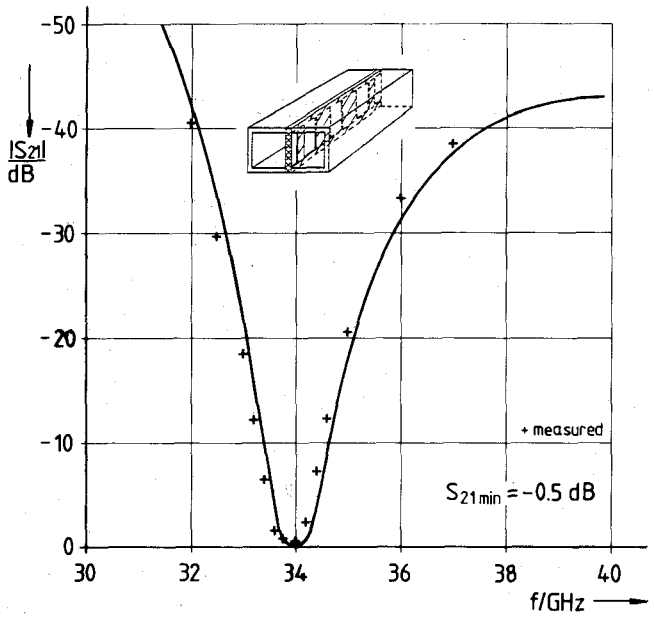

(a)

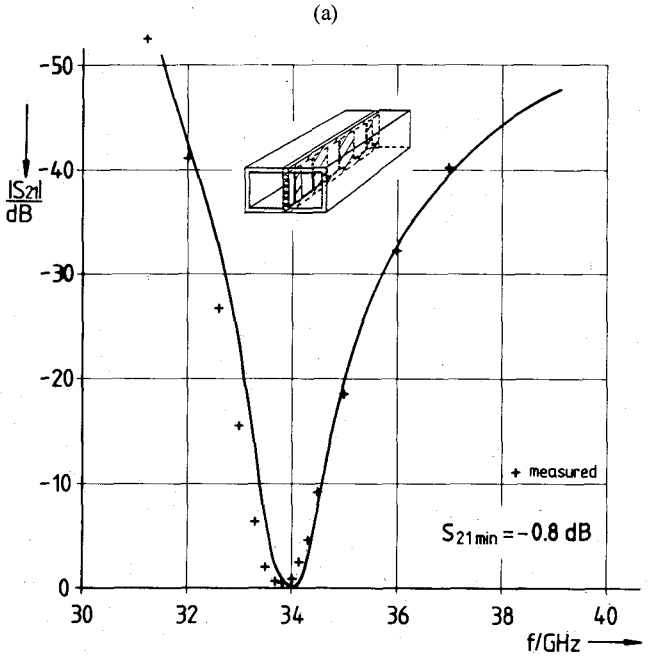

(b)

Fig. 4. Calculated and measured insertion loss of *Ku*-band fin-line filters (Table I). (a) Thickness of the dielectric substrate: 0.01 in. (b) Thickness of the dielectric substrate: 1/32 in.

The frequency displacement between the calculated and measured curves is caused by etching errors and production tolerances of the available material: copper cladding thickness about ± 2.5 μm, substrate thickness about ± 20 μm. This has been checked by using the measured geometry of the etched filters in the theory. Since the latter errors occur statistically, the displacements are towards both higher and lower frequencies.

The corresponding insertion losses of *Ka*-band fin-line filters with substrate thicknesses of 0.01 in and 1/32 in are given in Fig. 4. The calculated minimum insertion losses are about 0.3 dB, the measured values about 0.5 and 0.8 dB, respectively. For the thicker substrate, again, better

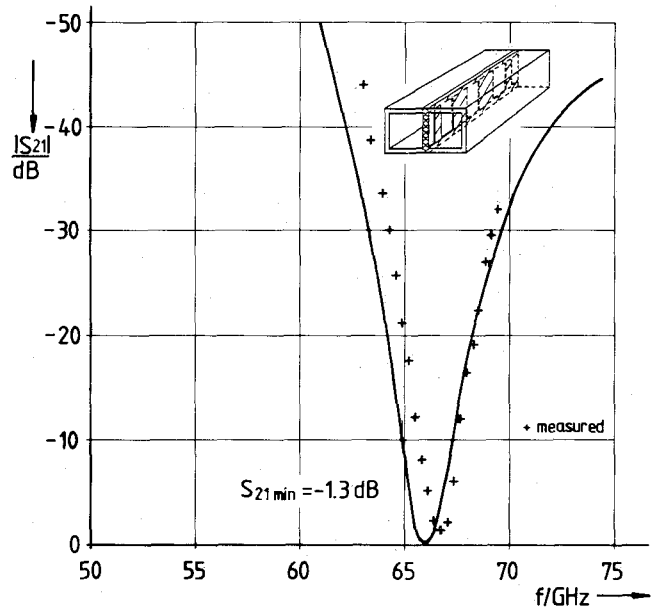

Fig. 5. Calculated and measured insertion-loss of a *V*-band fin-line filter (Table I). Thickness of the dielectric substrate: 0.005 in.

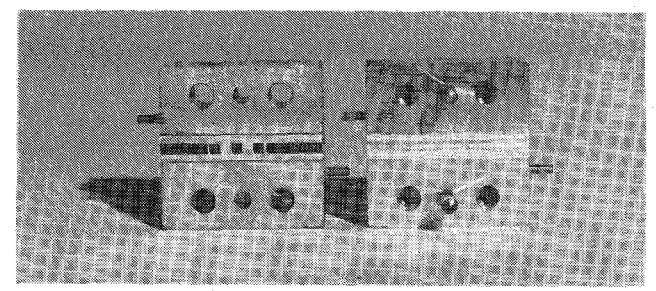

Fig. 6. Photoetched *V*-band fin-line structure (66.8 GHz).

stopband behavior is obtained.

Fig. 5 shows the calculated and measured insertion loss for a designed *V*-band fin-line filter (0.005-in thick dielectric substrate). The calculated minimum insertion loss is about 0.1 dB (versus the measured value of about 1.3 dB). The photoetched fin-line structure (*V*-band) is shown in Fig. 6.

V. Conclusion

A design theory has been described for low-insertion loss fin-line filters, consisting of alternating metallic bridges and gaps on a dielectric slab mounted between the broad walls of a rectangular waveguide. This theory includes higher order mode propagation, as well as the finite thicknesses of the dielectric slab and the metallic fins.

Three-resonator filters are chosen for design examples. The low-insertion loss design leads to measured passband insertion losses of about 0.25, 0.5, and 1.3 dB for the midband frequencies of about 15, 34, and 66 GHz, respectively. More resonators yield higher stopband attenuations and steeper characteristics but the insertion loss in passband is also higher (e.g., for a five-resonator filter by about 1.4 dB in *Ka*-band).

The low-insertion loss values result from the considerably higher unloaded Q of this filter resonators in compari-

son with the common small gap design and from the fact that no tapered transitions from waveguide to the fin-line structure are required. The second advantage, however, is neutralized if solid-state applications may necessitate small-gap integration and therefore suitable transitions to the $g/b=1$ structure. But since the additional insertion loss of constructed 20-mm long exponential double transitions ($g/b=1$ to $g/b=0.2$ and back to $g/b=1$) for the complete *Ka*-band was only typically about 0.5 dB, the low-loss fin-line filter design may still compare favorable with the small-gap design also for these applications.

A comparison of the characteristics of filters with different substrate thicknesses shows that thicker substrates provide better stopband attenuation, but because of the higher amount of energy propagated within the dielectric, the passband insertion-loss is also higher. RT/duroid 5880 is used for substrate material. To reduce losses and etching errors, fused silica (quartz) is suitable for further investigations because of its lower loss and surface roughness. Lower losses also result from a complete absence of supporting dielectrics.

Appendix

Abbreviations in (1)

$$\begin{bmatrix} f^{\mathrm{I}} \\ f^{\mathrm{II}} \\ f^{\mathrm{III}} \\ f^{\mathrm{IV}} \end{bmatrix} = \begin{bmatrix} x \\ d-\frac{e}{2}-x \\ a-x \\ x \end{bmatrix}$$

$$\begin{bmatrix} p^{\mathrm{I}} \\ p^{\mathrm{II}} \\ p^{\mathrm{III}} \\ p^{\mathrm{IV}} \end{bmatrix} = \begin{bmatrix} a \\ d-c-e \\ a-\left(d+\frac{e}{2}\right) \\ c-\frac{e}{2} \end{bmatrix}$$

$$\begin{bmatrix} k_{zm}^{\mathrm{I2}} \\ k_{zm}^{\mathrm{II2}} \\ k_{zm}^{\mathrm{III2}} \\ k_{zm}^{\mathrm{IV2}} \end{bmatrix} = k^{\nu 2} - \begin{bmatrix} \left(\frac{m\pi}{a}\right)^2 \\ \left(\frac{m\pi}{p^{\mathrm{II}}}\right)^2 \\ \left(\frac{m\pi}{p^{\mathrm{III}}}\right)^2 \\ \left(\frac{m\pi}{p^{\mathrm{IV}}}\right)^2 \end{bmatrix}, \qquad k^{\nu 2}=\omega^2\mu_0\epsilon_\nu.$$

Abbreviations in (5)

$$(W)=(E)-((U)+(E))^{-1}(V)((U)+(E))^{-1}(V)$$

(E) = unit matrix

$$(U)=\sum_{\nu=\mathrm{II}}^{\mathrm{IV}}\left[2(L)^{\nu}\left\{\left((E)-(R)^{\nu}(R)^{\nu}\right)^{-1}\left((N)^{\nu}\right)^{-1}\right\}-(L)^{\nu}\left((N)^{\nu}\right)^{-1}\right]$$

$$(V)=\sum_{\nu=\mathrm{II}}^{\mathrm{IV}}\left[2(L)^{\nu}\left\{\left((E)-(R)^{\nu}(R)^{\nu}\right)^{-1}(R)^{\nu}\left((N)^{\nu}\right)^{-1}\right\}\right]$$

$(R)^{\nu}$ = diagonal matrix of the three-waveguides structure with finite length l_2

$$(R)^{\nu}=\begin{bmatrix} e^{-jk_{z1}^{\nu}l_2} & \cdots 0 \\ \vdots & \ddots \\ 0 & e^{-jk_{zm}^{\nu}l_2} \end{bmatrix}$$

$$(N)^{\nu}:(N)^{\mathrm{II}}=(D_{Hmn})^{-1}(D_{Hnn})$$
$$(N)^{\mathrm{III}}=(D_{Hmk})^{-1}(D_{Hkk})$$
$$(N)^{\mathrm{IV}}=(D_{Hml})^{-1}(D_{Hll})$$

with the matrix coefficients

$$D_{Hmn}=k_{zm}^{\mathrm{I2}}A_m^{\mathrm{I}}H_{mn} \qquad D_{Hnn}=\frac{d-c-e}{2}k_{zn}^{\mathrm{II2}}A_n^{\mathrm{II}}$$

$$D_{Hmk}=k_{zm}^{\mathrm{I2}}A_m^{\mathrm{I}}H_{mk} \qquad D_{Hkk}=\frac{a-d-\frac{e}{2}}{2}k_{zk}^{\mathrm{III2}}A_k^{\mathrm{III}}$$

$$D_{Hml}=k_{zm}^{\mathrm{I2}}A_m^{\mathrm{I}}H_{ml} \qquad D_{Hll}=\frac{c-\frac{e}{2}}{2}k_{zl}^{\mathrm{IV2}}A_l^{\mathrm{IV}}$$

and coupling integrals

$$H_{mn}=\int_{x=c+e/2}^{d-e/2}\sin\frac{m\pi}{a}x\sin\frac{n\pi}{d-c-e}\left(d-\frac{e}{2}-x\right)dx$$

$$H_{mk}=\int_{x=d+e/2}^{a}\sin\frac{m\pi}{a}x\sin\frac{k\pi}{a-d-\frac{e}{2}}(a-x)\,dx$$

$$H_{ml}=\int_{x=0}^{c-e/2}\sin\frac{m\pi}{a}x\sin\frac{l\pi}{c-\frac{e}{2}}(x)dx.$$

$$(L)^{\nu}:(L)^{\mathrm{II}}=(D_{Emm})^{-1}(D_{Emn})$$
$$(L)^{\mathrm{III}}=(D_{Emm})^{-1}(D_{Emk})$$
$$(L)^{\mathrm{IV}}=(D_{Emm})^{-1}(D_{Eml})$$

with the matrix coefficients

$$D_{Emm}=\frac{a}{2}k_{zm}^{\mathrm{I}}A_m^{\mathrm{I}}$$
$$D_{Emn}=k_{zn}^{\mathrm{II}}A_n^{\mathrm{II}}H_{nm}$$
$$D_{Emk}=k_{zk}^{\mathrm{III}}A_k^{\mathrm{III}}H_{km}$$
$$D_{Eml}=k_{zl}^{\mathrm{IV}}A_l^{\mathrm{IV}}H_{lm}$$

and coupling integrals

$$H_{nm}=\int_{x=c+e/2}^{d-e/2}\sin\frac{n\pi}{d-c-e}\left(d-\frac{e}{2}-x\right)\sin\frac{m\pi}{a}x\,dx$$

$$H_{km}=\int_{x=d+e/2}^{a}\sin\frac{k\pi}{a-d-e/2}(a-x)\sin\frac{m\pi}{a}x\,dx$$

$$H_{lm}=\int_{x=0}^{c-e/2}\sin\frac{l\pi}{c-\frac{e}{2}}x\sin\frac{m\pi}{a}x\,dx.$$

Abbreviations in (11)

$$(W)=\left((E)-(Q_{22})(R)(Q_{22})(R)\right)^{-1}$$

$$R_{mm}=e^{-jk_{zm}l_1}.$$

Scattering coefficients of the single step

$$(Q_{11})=2(D_H)^{-1}(L_H)(M)-(E)$$

$$(Q_{21})=2(M)$$

$$(Q_{12})=2(D_H)^{-1}(L_H)(M)(D_E)^{-1}(L_E)$$

$$(Q_{22})=2(M)(D_E)^{-1}(L_E)-(E)$$

$$(M)=\left((D_E)^{-1}(L_E)+(D_H)^{-1}(L_H)\right)^{-1}$$

$$D_{Emm}=\frac{a}{2}k_{zm}^{I}A_m^{I}$$

$$D_{Hmm}=\frac{a}{2}k_{zm}^{I2}A_m^{I}.$$

The coefficients of the matrices (L_E) and (L_H) are given by

$$k_{zk}\left(A_k^{\mathrm{II}}\mathrm{I}_{mk}^{\mathrm{II}}+B_k^{\mathrm{II}}\mathrm{I}_{mk}^{\mathrm{II}'}+A_k^{\mathrm{III}}\left(-T_{1k}\mathrm{I}_{mk}^{\mathrm{III}}+\mathrm{I}_{mk}^{\mathrm{III}'}\right)+A_k^{\mathrm{IV}}\mathrm{I}_{mk}^{\mathrm{IV}}\right)=L_{Emk}$$

$$k_{zk}^2\left(A_k^{\mathrm{II}}\mathrm{I}_{mk}^{\mathrm{II}}+B_k^{\mathrm{II}}\mathrm{I}_{mk}^{\mathrm{II}'}+A_k^{\mathrm{III}}\left(-T_{1k}\mathrm{I}_{mk}^{\mathrm{III}}+\mathrm{I}_{mk}^{\mathrm{III}'}\right)+A_k^{\mathrm{IV}}I_{mk}^{\mathrm{IV}}\right)=L_{Hmk}$$

with the abbreviations

$$T_{1k}=\tan\left(k_{xk}^{\mathrm{III}}\cdot a\right).$$

Coupling integrals

$$\mathrm{I}_{mk}^{\mathrm{II}}=\int_{x=c+e/2}^{d-e/2}\cos\left(k_{xk}^{\mathrm{II}}x\right)\sin\left(\frac{m\pi}{a}x\right)dx$$

$$\mathrm{I}_{mk}^{\mathrm{II}'}=\int_{x=c+e/2}^{d-e/2}\sin\left(k_{xk}^{\mathrm{II}}x\right)\sin\left(\frac{m\pi}{a}x\right)dx$$

$$\mathrm{I}_{mk}^{\mathrm{III}}=\int_{x=d+e/2}^{a}\cos\left(k_{xk}^{\mathrm{III}}x\right)\sin\left(\frac{m\pi}{a}x\right)dx$$

$$\mathrm{I}_{mk}^{\mathrm{III}'}=\int_{x=d+e/2}^{a}\sin\left(k_{xk}^{\mathrm{III}}x\right)\sin\left(\frac{m\pi}{a}x\right)dx$$

$$\mathrm{I}_{mk}^{\mathrm{IV}}=\int_{x=0}^{c-e/2}\sin\left(k_{xk}^{\mathrm{IV}}x\right)\sin\left(\frac{m\pi}{a}x\right)dx.$$

References

[1] P. J. Meier, "Equivalent relative permittivity and unloaded Q-factor of integrated fin-line," *Electron. Lett.*, vol. 9, no. 7, pp. 162–163, Apr. 1973.

[2] P. J. Meier, "Integrated fin-line millimeter components," *IEEE Trans. Microwave Theory Tech.*, vol. MTT-22, pp. 1209–1216, Dec. 1974.

[3] P. J. Meier, "Millimeter integrated circuits suspended in the E-plane of rectangular waveguide," *IEEE Trans. Microwave Theory Tech.*, vol. MTT-26, pp. 726–732, Oct. 1978.

[4] D. Mirshekar-Syahkal and J. B. Davies, "Accurate analysis of tapered planar transmission lines for microwave integrated circuits," *IEEE Trans. Microwave Theory Tech.*, vol. MTT-29, pp. 123–128, Feb. 1981.

[5] A. M. K. Saad and K. Schünemann, "A simple method for analyzing fin-line structures," *IEEE Trans. Microwave Theory Tech.*, vol. MTT-26, pp. 1002–1007, Dec. 1978.

[6] A. M. K. Saad and K. Schünemann, "Design and performance of fin-line bandpass filters," in *Proc. 10th European Microwave Conf.*, (Warsaw), Sept. 1980 pp. 397–401.

[7] H. E. Hennawy and K. Schünemann, "Analysis of fin-line discontinuities," in *Proc. 9th European Microwave Conf.*, (Brighton), Sept. 1979, pp. 448–452.

[8] H. Hofmann, "Dispersion of planar waveguides for millimeter-wave application," *Arch. Elek. Übertragung*, vol. 31, pp. 40–44, 1977.

[9] A. Beyer, "Analysis of the characteristics of an earthed fin-line," *IEEE Trans. Microwave Theory Tech.*, vol. MTT-29, pp. 676–680, July 1981.

[10] A. Beyer and I. Wolff, "A solution of the earthed fin-line with finite metallization thickness," in 1980 *IEEE MTT-S Int. Microwave Symp. Dig.* (Washington, DC) pp. 258–260.

[11] L. P. Schmidt, T. Itoh, and H. Hofmann, "Characteristics of unilateral fin-line structures with arbitrarily located slots," *IEEE Trans. Microwave Theory Tech.*, vol. MTT-29, pp. 352–355, Apr. 1981.

[12] F. Arndt and U. Paul, "The reflection definition of the characteristic impedance of microstrips," *IEEE Trans. Microwave Theory Tech.*, vol. MTT-27, pp. 724–731, Aug. 1979.

[13] A. Hock and J. Rinderle, "Zur Anwendung der Evolutionsstrategie auf Schaltungen der Nachrichtentechnik," *Frequenz*, vol. 34, pp. 208–214, 1980.

[14] H. Schmiedel, "Anwendung der Evolutionsoptimierung bei mikrowellenschaltungen," *Frequenz*, vol. 35, 1981.

[15] Y. Konishi and K. Uenakada, "The design of a bandpass filter with inductive strip-planar circuit mounted in waveguide," *IEEE Trans. Microwave Theory Tech.*, vol. MTT-22, pp. 869–873, Oct. 1974.

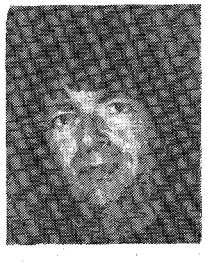

Fritz Arndt was born in Konstanz, Germany, on April 30, 1938. He received the Dipl.-Ing., the Dr.-Ing., and the Habilitation degrees from the Technical University of Darmstadt, Germany, in 1963, 1968, and 1972, respectively.

From 1963 to 1972 he worked on directonal couplers and microstrip techniques at the Technical University of Darmstadt. Since 1972 he has been a Professor of Microwave Engineering at the University of Bremen, Germany. His research activities are at present in the area of the solution of field problems of waveguide and fin-line structures, of antenna design, and of microwave holography.

Dr. Arndt is member of the VDE and NTG (Germany). In 1970 received the NTG award.

Jens Bornemann was born in Hamburg, West Germany, on May 26, 1952. He received the Dipl.-Ing. degree in electrical engineering in 1980 from the University of Bremen, West Germany.

Since 1980 he has been with the Microwave Department of the University of Bremen. His topics of interest include waveguide structures, discontinuity problems, and numerical techniques in electromagnetic theory.

Dietrich Grauerholz was born in Krems II, Germany, on September 22, 1945. He received the Dipl.-Ing. in 1971.

From 1971 to 1973 he worked in the High-Frequency Laboratory of Elektro-Spezial (Philips). In 1973 he joined the Microwave Department of the University of Bremen, where he has been engaged in the research and development of microstrip circuits, fin-line structures, and microwave measurements.

Rüdiger Vahldieck was born in Heiligenhafen, Germany, on July 8, 1951. He received his Dipl.-Ing. degree in electrical engineering from the University of Bremen, West Germany, in 1980.

His present research activities are in the field of microwave integrated circuits and in solving electromagnetic field problems for several waveguide discontinuities. Since 1980 he has been with the Microwave Department of the University of Bremen.

Radial-Symmetric *N*-Way TEM-Line IMPATT Diode Power Combining Arrays

DEAN F. PETERSON, MEMBER, IEEE

Abstract—**Circuit design and stability criteria are developed for a new class of IMPATT diode power combiners. These combiners make use of radial-symmetric circuits and provide an optimal integration of device and circuit properties to perform the power adding function. Both lossless *N*-way combiners and resistively stabilized *N*-way combiners are considered. Theoretical examples of this combining technique are given at *X*-band frequencies which make use of realistic experimentally determined IMPATT diode properties. Predictions for a 30-W ten-diode lossless *X*-band combiner indicate a 1-dB locking bandwidth of 300 MHz and 10-dB gain. A 100-W resistively stabilized 10-GHz ten-diode combiner predicts a 150-MHz locking bandwidth, also at 10-dB locking gain.**

I. Introduction

The purpose of this paper is to present a new approach to circuit-level power combining of negative-resistance devices in general and IMPATT diodes in particular. In a recent review article, the present state of microwave power combining techniques was effectively summarized by Russell [1], to which the reader is referred for an in-depth discussion of various combiner types and their performance. Basically, at the circuit level, combiners can be classified roughly into two categories: *N-way*, in which the outputs from all devices are combined in a single step, and *corporate* (hybrid) or *serial*, in which increasing power levels are successively combined. *N*-way combiners are often additionally separated into resonant and nonresonant structures. Examples of the former are the waveguide combiner of Kurokawa and Megalhaes [2] and the circular cylindrical TM_{0n0} cavities of Harp *et al.* [3]–[6]. Examples of the nonresonant *N*-way combiner include the nonplanar Wilkinson hybrid [7] and the five-way combiner of Rucker [8].

Each of these power combining circuits has its associated performance limitations, design criteria, and problems. Corporate or serial combiners have the advantage of isolation between devices to eliminate deleterious interactions and provide broadband performance, but have the disadvantage of often substantial circuit and combining losses [1], often at high power levels. Resonant *N*-way combiners require stabilization resistors to suppress interactions among devices and undesired oscillation modes in a high-*Q* cavity, leading to narrow-band although high-efficiency combining. Nonresonant *N*-way structures usually provide larger bandwidths with a corresponding increase in the mode suppression problem. Rucker's technique [8] analyzed by Kurokawa [9] has been successful, as has apparently been a conical line technique [10]. Radial arrays of equally spaced TEM lines have been used successfully for transistor power combining [11].

The combining circuits treated in this paper could perhaps be classified as *N*-way nonresonant transmission-line networks. As opposed to other networks of this type, however, the "circuit" and "device" properties are closely intertwined such that each cannot be specified independently. Hence the combiner represents, in some sense, an optimal integration of device and circuit to perform the power adding function. Both lossless and resistively stabilized symmetrical combining circuits are considered and each can provide the desired suppression of the unwanted non-power-producing modes while affording design flexi-

Manuscript received July 2, 1981; revised August 31, 1981. This work was supported by the Air Force Avionics Laboratory, Wright-Patterson Air Force Base, under Contract F33615-77-C-1132.

The author is with the Electron Physics Laboratory, Department of Electrical and Computer Engineering, University of Michigan, Ann Arbor, MI 48109.

0018-9480/82/0200-0163$00.75 ©1982 IEEE